Cyclopentadiene-based hole-transport material for cost-reduced stabilized perovskite solar cells with power conversion efficiencies over 23%

Michael Bauer,‡ Hongwei Zhu,‡ Yuhang Liu,* Christoph Lorenz, Elena Mena-Osteritz, Dirk Hertel, Shaik Mohammed Zakeeruddin, Klaus Meerholz, Michael Grätzel* and Peter Bäuerle*

M. Bauer, C. Lorenz, Dr. E. Mena-Osteritz, Prof. P. Bäuerle
Institute of Organic Chemistry II and Advanced Materials, University of Ulm, Albert-Einstein-Allee 11, 89081 Ulm, Germany.
E-mail: peter.baeuerle@uni-ulm.de

H. Zhu,§ Dr. Y. Liu, Dr. S. M. Zakeeruddin, Prof. M. Grätzel
Laboratory of Photonics and Interfaces, Institute of Chemical Sciences and Engineering, École Polytechnique Fédérale de Lausanne (EPFL), Station 6, 1015 Lausanne, Switzerland.
E-mail: michael.graetzel@epfl.ch

Dr. D. Hertel, Prof. K. Meerholz, Department of Chemistry, University of Cologne, Greinstr. 4-6, 50939 Cologne, Germany.
E-mail: klaus.meerholz@uni-koeln.de

§Current address: H. Zhu, School of Chemical Engineering and Technology, Tianjin University, Tianjin 300072, China.

‡ These authors contributed equally to this work

Abstract

Hole transport materials (HTM) are an important component in perovskite solar cells (PSC). Despite a multitude of HTMs have been developed in recent years, only few of them lead to solar cells with efficiencies over 20%. Therefore, it is still a challenge to develop high-performing HTMs, which have ideal energy levels of the frontier orbitals, are highly efficient in transporting charges, and stabilize the solar cell at the same time. In this work, we describe the development of a structurally novel molecular HTM, **CPDA 1**, which is based on a common cyclopentadiene core and can be efficiently and inexpensively synthesized from readily available starting materials which is important for future realization of low-cost PV on larger scale. Due to excellent optoelectronic, thermal, and transport properties, **CPDA 1** not only meets the envisioned properties by reaching high efficiencies of 23.1%, which is among the highest reported to date, but also contributes to a respectable long-term stability of the PSCs.

1. Introduction

Hybrid organic-inorganic metal halide perovskite have attracted much interest as light-absorbing materials in solar cells due to their excellent optoelectronic properties such as low exciton binding energy, high absorption coefficients, and high charge carrier diffusion length combined with straightforward preparation process.[1-6] Power conversion efficiencies (PCE) of perovskite solar cells (PSC) have been improved from 3.8% in 2009[7] to close to 25% nowadays.[8] Herewith, the top-notch materials for PSCs outperform CIGS, CdTe, and polycrystalline silicon and are now approaching monocrystalline silicon.[9]

In high performance mesoscopic PSCs with common n-i-p layer structure, the hole-transport material (HTM), which is sandwiched between the photoactive ammonium or amidinium lead halide and the back collector, represents a key component. HTMs play a major role not only in hole extraction and transport and in blocking of electrons, but also act as a stabilizing capping layer for air and moisture protection on the photoactive perovskite.[10,11] Within the scope of more stable and highly efficient perovskite absorbers, a wide range of HTMs has been developed including organic polymeric, metal organic, and the widely applied molecular organic HTMs. Recent reviews well describe strategies for the successful design and synthesis of such high performance HTMs.[12-14] These are also thought to surpass the globally used and well-explored "gold-standard" HTM, spiro-OMeTAD,[15] which exhibits some unfavorable properties, including limited long-term stability, high cost, and moderate hole mobility.[16]

For the structural or molecular design of attractive and efficient HTMs a multi-parameter problem should be taken into account. Besides excellent hole mobility other crucial properties need to be met: (*i*) high solubility in common organic solvents for processing of uniform thin layers; (*ii*) high chemical and light stability; (*iii*) high morphological and thermal stability; (*iv*) high hydrophobicity and moisture

stability; (*v*) avoidance of additives and dopants, which increase the hole concentration, but introduce detrimental destabilizing hydrophilicity, and finally (*vi*) straightforward synthesis strategies allowing for up-scaling and reduced manufacturing costs by minimizing synthetic steps and purification procedures.[12] All these factors contribute for the transition of HTMs from academia to industrial commercialization of highly efficient and stable low-cost PV.[17]

Various molecular concepts have been employed in the search and synthesis of new molecular organic HTMs, most of them comprise triphenylamine units due to their low ionization potential and HOMO energy level. The propeller-like arrangement of the phenyl residues opts for a more favorable amorphous phase in the films. Only few PSCs comprising current HTMs surpass or come close to the 24.0% efficiency of the best spiro-OMeTAD-based PSCs.[18] The complex spiro concept, in which two π-conjugated moieties are connected via a sp^3-carbon, was very recently used by Yang *et al*. by synthesizing fluorinated variants of spiro-OMeTAD, which as HTM contributed to record PCE of 24.8% (reverse scan) and 23.9% (average) in PSCs surpassing spiro-OMeTAD (PCE 22.7%) measured under identical conditions.[8] Seo *et al.* replaced phenyl rings of spiro-OMeTAD by more extended fluorene units and achieved PCEs of 23.2% (reverse scan) and 22.9% in steady state.[19] Very recently, we have developed a new stable HTM comprising a central spiro-acridine cyclopentadithiophene-core flanked with triarylamine moieties. Best performing PSCs yielded PCEs of 21.1% and excellent long-term operational stability. This HTM exhibited a higher hole mobility, higher thermal, and better moisture stability as compared to spiro-OMeTAD.[20] Other structural concepts employ star-shaped or dendritic arrangements of triarylamine moieties. In this respect, Liao *et al.* prepared HTMs having an indolocarbazole core comprising three symmetrical diphenylamine arms and achieved 21.6% PCE in PSCs.[21] Guo *et al.* straightforwardly prepared a linear triphenylamine donor-acceptor HTM including an anchoring group. Corresponding PSCs achieved PCEs of up to 21.2% and the HTM was processable from non-chlorinated solvents.[22]

Herein, we disclose the development of novel HTM **CPDA 1**, which comprises **c**yclo**p**enta**d**iene dimethyl **a**cetale as a new structural core element for HTMs flanked by four triarylamine arms in a star-shaped fashion. Very thin layers of **CPDA 1** resulted in high efficiencies of 23.1% (reverse scan) and 23.0% (average) in n-i-p PSCs surpassing spiro-OMeTAD (21.9% average) in various metrics mentioned above, among them straightforward inexpensive synthesis, higher efficiency, smaller hysteresis of the *J-V* curves, and substantially higher long-term stability in PSCs.

2. Results and discussion

2.1 Synthesis of new HTM CPDA 1

HTM **CPDA 1** was synthesized in one step and 77% yield in a fourfold Suzuki-type Pd-catalyzed cross-coupling reaction of tetrabromocyclopentadiene dimethyl acetale **2** and triarylamine boronic ester **3**

(**Scheme 1**). Dimethyl acetale **2** was efficiently prepared in two steps and boronic ester **3** in three steps according to literature procedures (Supporting Information, SI). The elaborated synthetic procedure over six steps delivered CPDA **1** in good overall yield of 52% starting from aniline and other very low priced reagents such as cyclopentadiene and *p*-iodoanisole which clearly allow for efficient up-scaling. A cost estimation for the preparation of HTM **CPDA 1**, which includes only commercial prices for the starting materials, resulted in a substantially reduced price compared to spiro-OMeTAD[22] (**Table S1**, SI). The structure of **CPDA 1** was confirmed by ^{1}H- and ^{13}C-NMR-spectroscopy (**Figure S1**, **S2**, SI) and high resolution mass spectra (HRMS) (**Figure S3**, **S4**, SI).

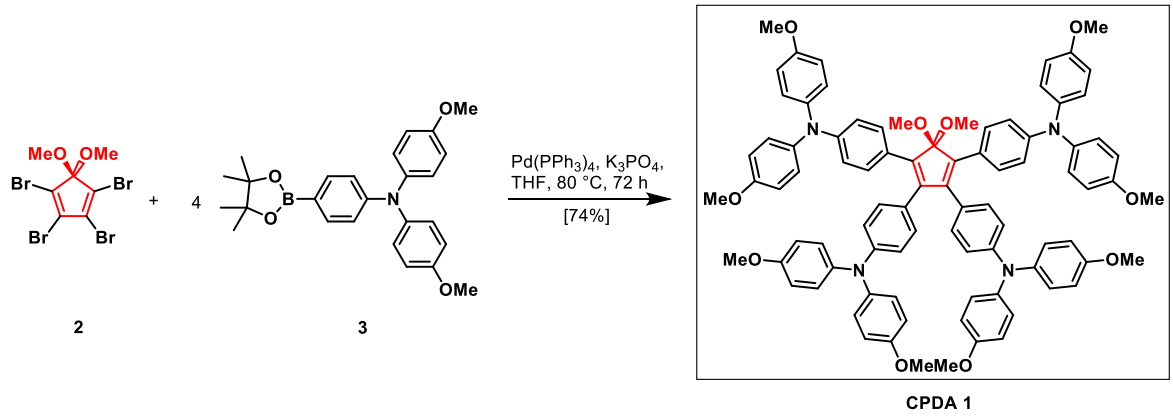

Scheme 1. Synthesis of novel hole-transport material **CPDA 1**.

2.2 Single crystal X-ray structure analysis

We were able to grow single crystals of **CPDA 1** suitable for X-ray diffraction measurement, which is important for the determination of the packing motif and distances of the molecules in the solid state. Crystals were obtained by antisolvent vapor-assisted crystallization by slow diffusion of *n*-hexane into a dichloromethane solution of **CPDA 1** and belong to the triclinic space group $P\,\overline{1}$. Key parameters of the crystal structure refinement are summarized in **Table S2** (SI). The unit cell (a = 10.8185(2) Å, b = 16.2139(5) Å, c = 22.5926(6) Å; α = 107.709(3)°, β = 95.3396(19)°, γ = 90.349(2)°) contains two equivalent molecules (**Figure S5**, SI) and selected molecular bond lengths, angles, and torsion angles are compiled in **Tables S3**, **S4**, **S5**, and **Figure S6** (SI). In **Figure 1** the molecular geometry of **CPDA 1** including torsion angles between the inner phenylene rings and the central cyclopentadiene dimethyl acetale core is shown in front and side view. The inner phenylene rings of the four triarylamine substituents attached at the 2,5-position of the CPDA unit showed rather small torsion angles of around 11.5° whereas the respective phenylenes at the 3,4-positions are strongly distorted from planarity by 65° and 109° (**Figure 1**, top). As a consequence, the corresponding bond lengths are shorter for the 2,5-connection (1.464 Å and 1.458 Å) compared to the 3,4-substitution (1.481 Å and 1.479 Å) indicating a

higher π-conjugation in this pathway. The spiro-carbon of the central CPDA unit is nearly ideally tetrahedral and the methoxy groups are only slightly distorted by 2-7° (**Figure 1**, bottom).

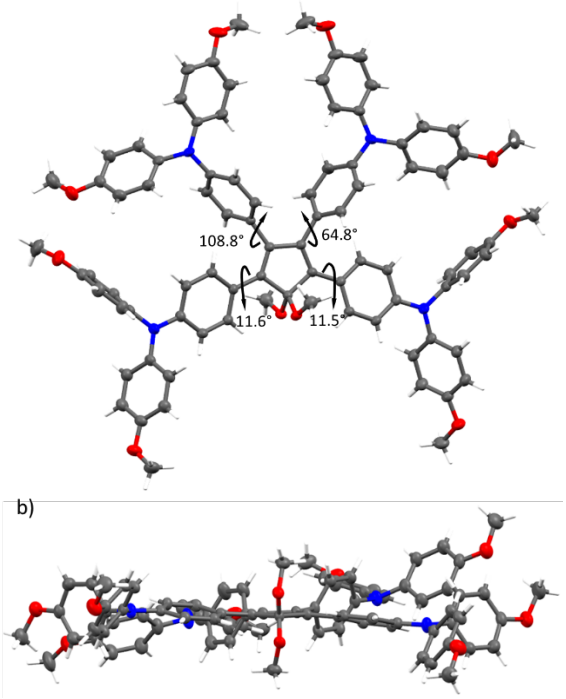

Figure 1. Single crystal X-ray structure analysis of **CPDA 1** showing the molecular geometry comprising torsion angles between the inner phenyl rings and the central cyclopentadiene dimethyl acetale core unit (top) and side view (bottom).

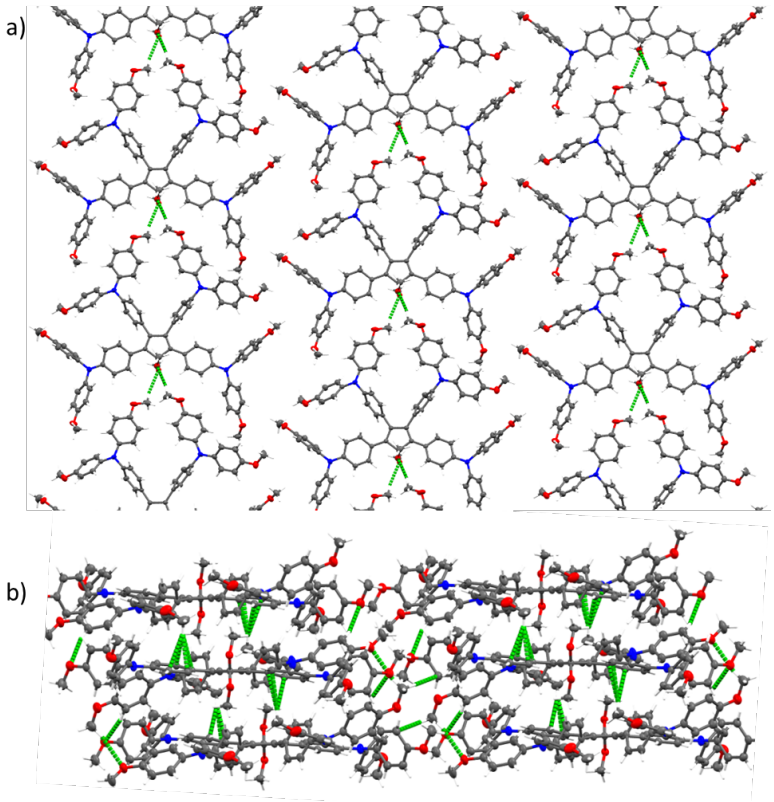

Figure 2. Packing motif of **CPDA 1** showing intermolecular short contacts (green lines) between atoms perpendicular to a) and along b) the (-101) plane dominated by CH---O andCH---C interactions (green dotted lines). Solvent molecules have been omitted for clarity.

The molecular packing motif of **CPDA 1** in the (-101) plane is dominated by CH---O interactions of methoxy groups (**Figure 2**, top). In the perpendicular direction several CH---C and CH---O intermolecular interactions stabilize the antiparallel oriented molecules in the adjacent planes (**Figure 2**, bottom). All short contacts involve hydrogen atoms in herringbone-type interaction lacking evidence of π–π stacking (**Table S6**, **S7**, SI).

2.3 Thermal properties

Differential scanning calorimetry (DSC) was used to determine thermal properties of the HTM which are important for processing temperatures and long-term stability of the photovoltaic devices. **CPDA 1** revealed in the first scan a sharp melting point at 266 °C. No crystallization occurred in the back scan. The second heating scan showed a glass transition temperature (T_g) at 120 °C (**Figure 3**a) which is identical to that of amorphous spiro-OMeTAD.[15] Further heating indicated exothermic crystallization in the range of 170–205 °C (supported by optical microscopy), and finally a broad melting point peaking at 257 °C was identified.

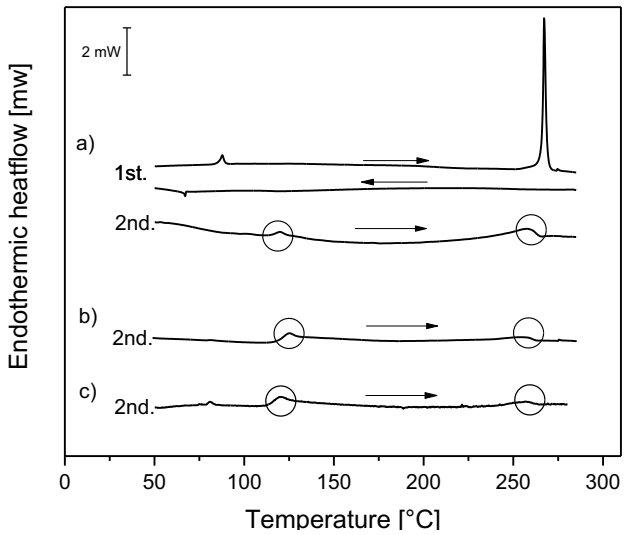

Figure 3. *a)* DSC of CPDA **1**, first scan and second heating scan. *b)* DSC of **CPDA 1** and additive lithium bis(trifluoromethansulfonyl) imid (LiTFSI) (15.1 : 1, w/w), second heating scan. *c)* DSC of **CPDA 1** and additives LiTFSI and 4-*tert*-butylpyridine (4-*t*BP) (15.1 : 1 : 4.6, w/w/w), second heating scan. For all measurements a heating rate of 10 °C/min was used and 1 min isothermal equilibration after each measurement. The second heating scans are enhanced by a factor of 3.

In order to investigate the phase transition behavior and thermal stability of the operative photoactive layer in the solar cells, DSCs of **CPDA 1** containing additives lithium bis(trifluoromethanesulfonyl) imid (LiTFSI) and 4-*tert*-butylpyridine (4-*t*BP) were measured (details see captions **Figure 3**). Interestingly, T_g (120–125 °C) and melting point (257 °C) of **CPDA 1** were only marginally influenced by the

additives (**Figure 3**b,c), while the T_g of doped spiro-OMeTAD drops to ~70 °C[23] which can be harmful for PSCs at operational conditions. HTM **CPDA 1** is thermally stable and decomposition, which is expected to involve the loss of a methoxy group, started at a temperature of 280 °C (5% mass loss) measured by thermal gravimetric analysis (TGA) (**Figure S7**, SI).

2.4 Optoelectronic properties

The optical properties of **CPDA 1** were investigated by UV-vis and fluorescence spectroscopy in dichloromethane solution (**Figure 4**, left). The absorption spectrum showed a strong absorption band with a maximum at λ_1 = 304 nm (ε = 75 000 M^{-1} cm^{-1}) and two weaker bands at λ_2 = 396 nm (ε = 29 800 M^{-1} cm^{-1}) and λ_3 = 454 nm (ε = 27 300 M^{-1} cm^{-1}). In order to understand the complex absorption behavior, we split the molecule into various sub-chromophores. We assign the strongest high-energy absorption to the triarylamine chromophores in accordance with bis(4-methoxyphenyl)amine, which shows an absorption maximum at 298 nm (ε = 23 000 M^{-1} cm^{-1}).[24] Another reasonable chromophore is represented by the 4,4'-bis(4-methoxyphenyl)stilbene unit, which as *trans*-isomer shows two absorption bands at 398 nm and 305 nm in accordance with λ_2 and λ_1 of **CPDA 1**.[25] It is long known for cyclopentadienone acetales that in comparison to the corresponding cyclopentadienes the longest wavelength band is bathochromically shifted due to spiro-conjugation.[26,27] Therefore, we assign the band at lowest energy at 454 nm in the absorption spectrum of CPDA **1** to the spiro-conjugated cyclopentadiene acetale structure. The absorption onset corresponds to an optical energy gap of 2.37 eV. An emission maximum is found at 577 nm (2.15 eV; **Figure 4**, left). The corresponding absorption maxima of thin films of **CPDA 1** are not or only marginally red-shifted (λ_1 = 304 nm, λ_2 = 402 nm, λ_3 = 460 nm, E_g = 2.30 eV) indicating rather amorphous character and very low degree of aggregation (**Figure S8**, SI).

The redox properties of **CPDA 1** were investigated by means of cyclic voltammetry (CV) in tetrabutylammonium hexafluorophosphate ($TBAPF_6$)/dichloromethane as electrolyte and potentials were referenced against the redox couple ferrocene/ferricenium (Fc/Fc^+). The time semi-derivative convolution of the cyclic voltammogram of **CPDA 1** showed reversible oxidation waves at 0.02 V and 0.08 V, which are only slightly separated, at 0.38 V, and a quasireversible wave at 1.00 V (**Figure 4**, right). The determination of the transferred electrons by redox titration revealed a ratio of 1:1:2:4 indicating that two triarylamine moieties are firstly consecutively oxidized to the radical cation (first two waves), then subsequently the other two (third wave). The fourth wave reflects the simultaneous further oxidation of all four triarylamine units to the dications. The highest occupied molecular orbital (HOMO) energy level of -5.04 eV for **CPDA 1** was calculated from the onset of the first oxidation wave assuming a value of -5.1 eV for Fc/Fc^+ vs vacuum[28] and is identical to that of spiro-OMeTAD. UPS measurement on thin

films of CPDA **1** yielded an identical value of -5.03 eV. The favorable HOMO level will benefit efficient hole-extraction from perovskite active layer to HTL.

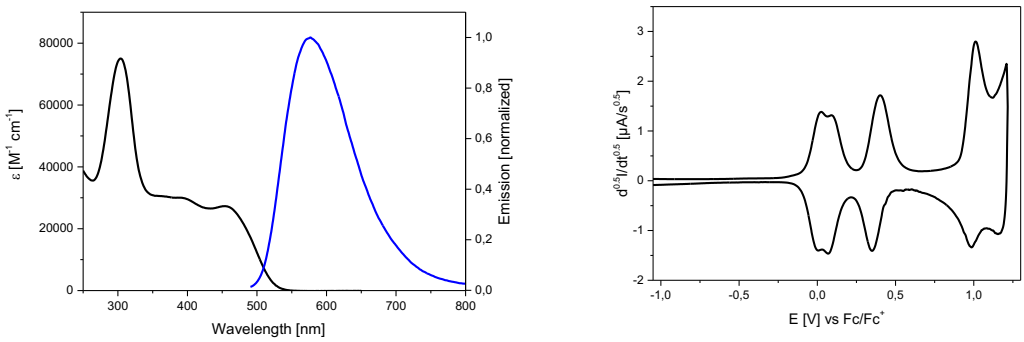

Figure 4. Absorption spectrum (black curve, c= 5.0 x 10^{-5} M) and emission spectrum (blue curve, c= 1 x 10^{-7} M) of **CPDA 1** in dichloromethane (left). Time semi-derivative deconvolution of a cyclic voltammogram of **CPDA 1** in dichloromethane/TBAPF (0.1 M), c = 5 x 10^{-4} mol/L, scan speed 100 mV/s, room temperature, referenced against the ferrocene/ferricenium couple (Fc/Fc^+) (right).

2.5 Mobility and time-resolved photoluminescence measurements

The hole mobility of pristine HTM layers was determined by time-of-flight (ToF) measurements. A hole mobility μ_h of about 2 · 10^{-4} cm^2/Vs at an applied field of 2.5 · 10^5 V/cm ($E^{1/2}$ = 500 $(V/cm)^{1/2}$) was determined for reference compound spiro-OMeTAD consistent with an earlier report (**Figure 5**).[20,29] The extrapolated zero-field mobility $\mu_{h,0}$ corresponds to 1 · 10^{-5} cm^2/Vs. By contrast, **CPDA 1** showed a lower hole mobility, specifically $\mu_h \approx 3 \cdot 10^{-5}$ cm^2/Vs at an applied field of 2.5 · 10^5 V/cm and $\mu_{h,0}$ = 6 · 10^{-6} cm^2/Vs, respectively. In both cases, the ToF signals are characteristic of equilibrium hole transport, indicative of trap-free transport. To support this conclusion, we measured ToF on samples with varying thickness (**Figure S9**, SI) and obtained the same mobility within experimental error.

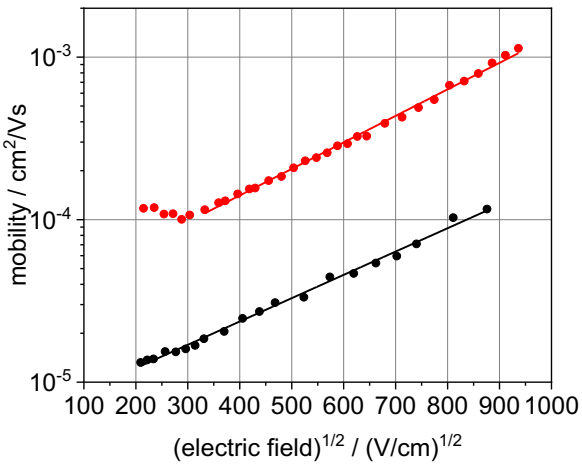

Figure 5. Field-dependent hole mobility obtained by ToF measurements for spiro-OMeTAD (red) and **CPDA 1** samples (black). The lines a fit to the data.

The obtained ToF mobility values were further verified by space-charge limited current (SCLC) measurements on non-doped devices. Hole mobilities of doped films of **CPDA 1** in comparison to spiro-OMeTAD were as well measured by the SCLC method in hole-only devices, with the same dopant concentrations of LiTFSI and4-*t*BP as used in corresponding PSC devices. The current density versus bias voltage curves are shown in **Figure S10** (SI) and hole mobilities were obtained by fitting the results to the Mott-Gurney law for space charge limited current. In this manner, for novel HTM **CPDA 1** a hole mobility of $\mu_h \approx 2.4 \cdot 10^{-4}$ cm^2/Vs was determined which is more than double compared to spiro-OMeTAD ($\mu_h \approx 1 \cdot 10^{-4}$ cm^2/Vs). Thus, SCLC data on doped devices as typically used in solar cells indicate an inverse behaviour compared to the pristine films and **CPDA 1** exhibited a higher hole mobility compared to spiro-OMeTAD which should be beneficial for efficient hole-transport and consequently for the solar cell performance in PSCs.

The potential for high performance of **CPDA 1** in PSCs was firstly verified by time-resolved photoluminescence (TRPL) in order to obtain insight of hole extraction in comparison to spiro-OMeTAD (**Figure 6**). Three different regimes in the TRPL traces measured at low fluences (<4 nJ/cm^2) can be observed. We follow the interpretation given in Kirchartz *et al*.[30] The rapid decay within the first 10 ns is dominated by charge carrier diffusion after the initial laser-induced exponential carrier profile. After this an exponential decay until ~70 ns is observed which comes mainly from hole transfer from the perovskite into the HTM. At later times, the TRPL trace is dominated by interface recombination. The TRPL traces for both HTMs are very similar but we observe a slight difference in the second time regime form 10-70 ns. To quantify this difference, we applied numerical simulations to model the TRPL traces for times <70 ns, the details of these simulations have been described in our previous work.[4] We modeled a hole-transfer velocity of 700 cm/s for the perovskite/spiro-OMeTAD and 900 cm/s for the perovskite/**CPDA 1** interface resulting in a slightly better hole extraction capability for **CPDA 1**.

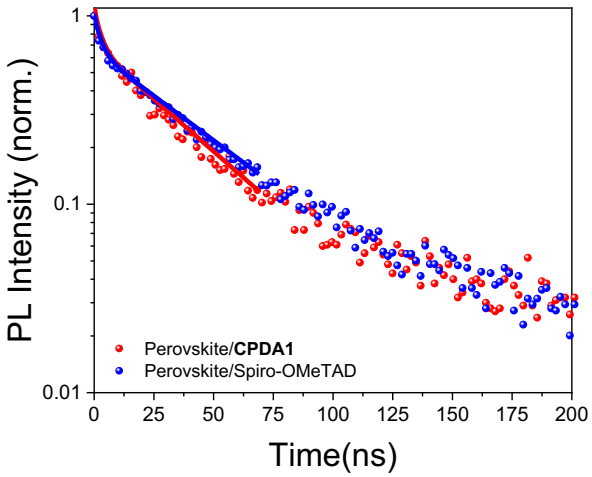

Figure 6. TRPL decay of perovskite films coated with different HTM. The solid lines indicate the model fits.

2.6 Photovoltaic properties and solar cell performance

To investigate the potential application of **CPDA 1** in solar cells, PSCs are fabricated with a standard structure of glass/FTO/compact-TiO_2/mesoscopic-TiO_2/perovskite/HTM/gold (**Figure 7**A, B), in which an iodide-rich perovskite recipe $FA_{0.85}MA_{0.1}Cs_{0.05}Pb(I_{0.97}Br_{0.03})_3$ was used. The current density-voltage (*J-V*) curves of devices based on **CPDA 1** (black curve) and spiro-OMeTAD (red curve), measured under AM1.5G irradiation are displayed in **Figure 7** and the corresponding photovoltaic parameters summarized in **Table 1**. A champion cell with a PCE of 23.1% was fabricated using **CPDA 1** as HTM. This device produced a V_{oc} of 1099 mV, a fill factor (FF) of 82.1%, and a J_{sc} of 25.6 mA cm^{-2}. PSCs using spiro-OMeTAD as HTM and the same perovskite recipe for reference, gave a slightly lower PCE of 22.6%. The **CPDA 1**-based device was scanned in both, reverse (RVS) and forward (FWS) way, and the obtained PV parameters showed less hysteresis compared to PSCs with spiro-OMeTAD as HTM. The observed slight outperformance of **CPDA 1**-based PSC is in agreement with the aforementioned results obtained from SCLC hole mobility and TRPL experiments, together with reduced HTL thickness for **CPDA 1**.

The stabilized power output at the maximum power point (MPP) stability of champion PSCs with **CPDA 1** and spiro-OMeTAD were monitored under dehumidified ambient air (10% RH). Within the first 5 min, **CPDA 1**-based PSC presents a stable power output of 22.98% (see inset of **Figure 7**C), which is approaching the PCE obtained from backward *J-V* scan. However, the output PCE of spiro-OMeTAD-based PSC decrease from 22.50% to 21.87%, implying better operational stability of devices based on **CPDA 1** due to a higher T_g that is not affected by dopants. The incident photon-to-current conversion efficiencies (IPCE) of the champion devices based on **CPDA 1** and spiro-OMeTAD are shown in **Figure 7**D. The integrated photocurrents are in good agreement with the corresponding J_{sc} values measured from *J-V* curves (Table 1). Standard deviations and statistics of the photovoltaic parameters V_{oc}, J_{sc}, FF, and PCE are shown in **Figure 7**E.

Table 1. PV parameters of PSCs based on HTM **CPDA 1** in comparison to spiro-OMeTAD

Hole-transport material	V_{oc}	J_{sc} [c] [mA/cm^2]	J_{sc} [d] [mA/cm^2]	FF [%]	PCE [e] [%]	PCE [f] [%]
CPDA 1 [a]	1.099	25.60	24.98	0.821	23.10	22.98
CPDA 1 [b]	1.093	25.61		0.816	22.84	
spiro-OMeTAD [a]	1.091	25.54	24.78	0.810	22.57	21.87
spiro-OMeTAD [b]	1.081	25.56		0.805	22.24	

a) Reverse scan; b) forward scan; c) J_{sc}determined from the *J-V* measurement; d) J_{sc}determined from IPCE; e) PCE determined from *J-V* measurement; f) PCE determined from 300 s MPP tracking.

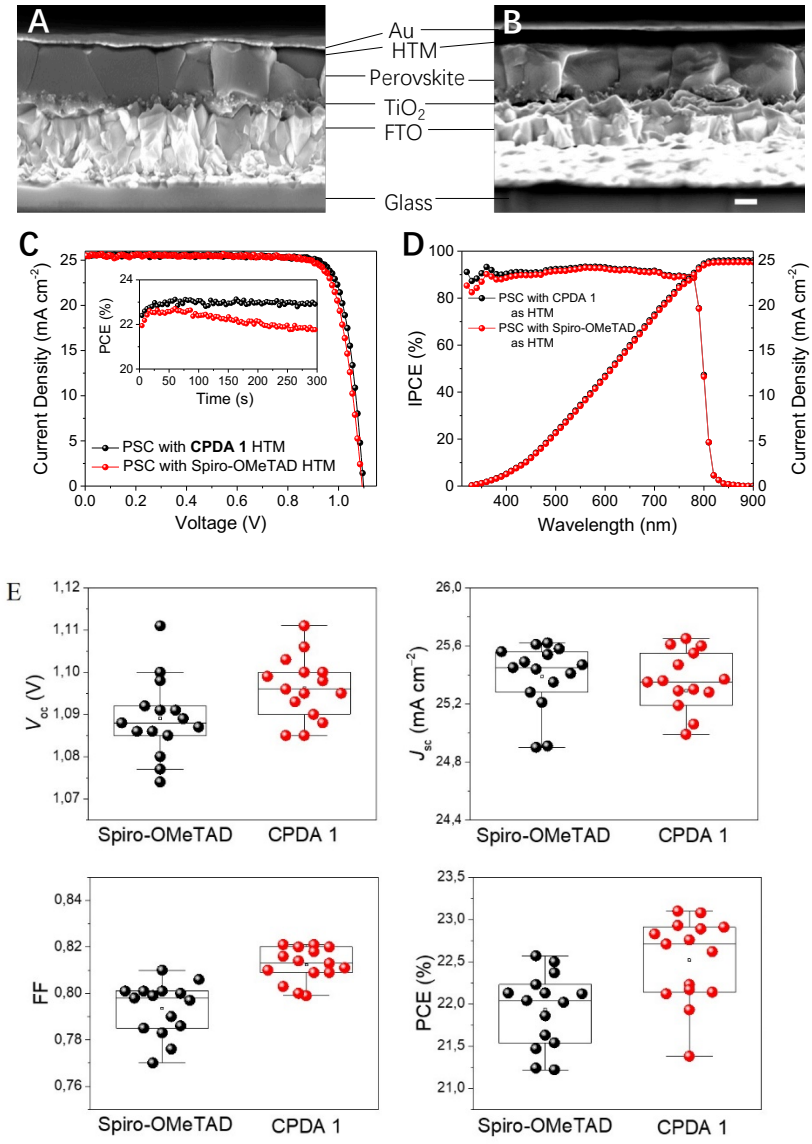

Figure 7. PSC device characterizations. Cross-sectional SEM photos of PSCs with **A**, **CDPA 1** as HTM and **B**, spiro-OMeTAD as HTM, the scale bar represents 200 nm, **C**, *J-V* curves of PSCs with **CPDA 1** and spiro-OMeTAD as HTM with the inset showing stable outputs of both PSC devices and **D**, IPCE curves and integrated photocurrent of PSCs with **CPDA 1** or spiro-OMeTAD as HTMs, **E** Device statistics and standard deviations of the photovoltaic parameters V_{oc}, J_{sc}, FF, and PCE. Distributions of 15 devices obtained from spiro-OMeTAD and CPDA **1** based devices fabricated in one batch.

Operational stability for devices based on **CPDA 1** and spiro-OMeTAD without encapsulation was investigated under 1 sun irradiation and under nitrogen atmosphere (N_2). The results are shown in **Figure 8**. After 500 hours, the device based on **CPDA 1** as HTM retained 90% of its initial efficiency, in contrast to 65% for the one with spiro-OMeTAD. In addition, a fast decay within the first 50 hours up to 18% (*burn-in*) was observed which is in agreement with the power output measurement as shown in **Figure 8**A. **CPDA 1**-based PSCs exhibited superior operational stability as compared to spiro-OMeTAD, which potentially is of great importance for further industrial application for advanced PSC techniques. Due to the reduced hydrophilic dopant lithium bis(trifluoromethanesulfonyl)imide (LiTFSI) and

tert-butyl pyridine (4-*t*BP) that is introduced into **CPDA 1** HTL-layers, we anticipate better moisture resistivity of **CPDA 1**-based PSCs as compared to spiro-OMeTAD. In this respect, we firstly performed contact angle measurement for perovskite film coated with **CPDA 1** or spiro-OMeTAD (**Figure 8**B). An increased contact angle from 69.6° to 85.1° for **CPDA 1**-based sample as compared to spiro-OMeTAD was observed. Additionally, we also monitored the stability of PSCs based on both HTMs stored in ambient with an RH (relative humidity) of 40-60% (**Figure 8**C). We attribute the better stability for PSC based on **CPDA 1** to less moisture uptake that is related to the minor amount of hydrophilic dopant. PSCs based on spiro-OMeTAD generally exhibit poor stability under heat stress due to the lowered T_g after doping.

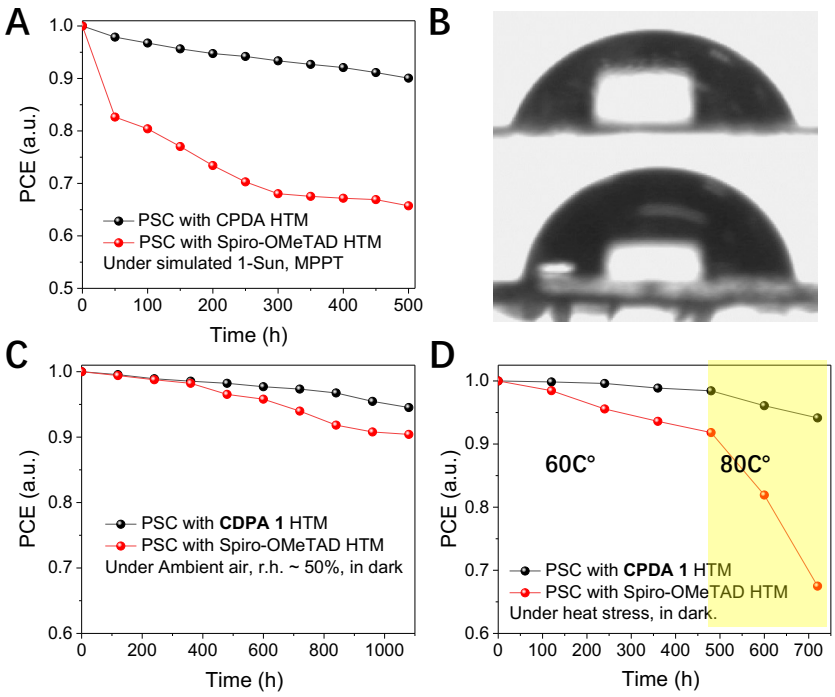

Figure 8. A) Maximum power point (MPP) ageing results in inert atmosphere (N_2) and under 1 sun continuous illumination of PSCs with **CPDA 1** and spiro-OMeTAD as HTM. B) Images of water droplets on the surface of a perovskite film coated with **CPDA 1** and spiro-OMeTAD and PSC 'shelf life' stability under stress of C), moisture and D) heat stress.

We monitored herewith long-term stability of **CPDA 1**-based PSCs in comparison to spiro-OMeTAD devices by applying various temperatures. At an ageing temperature of 60 °C both PSCs exhibited good stability. In this line, **CPDA 1**-based PSCs showed practically no decay of PCE after 470 h and those with spiro-OMeTAD less than 10%. While at an elevated temperature of 80 °C, PSCs with **CPDA 1** as HTM were still quite stable and showed a drop of efficiency of only ~10% after 250 hours, PCE dropped significantly by ~30% for spiro-OMeTAD-based devices due to the low T_g of doped spiro-OMeTAD (<80 °C). Therefore, spiro-OMeTAD films suffered from glass transition-related deformation, while the

higher T_g (120 °C) of **CPDA 1** assured minor degradation by forming a robust film against heat stress (**Figure 8**D).

3. Conclusions

In conclusion, we reported on straightforward and inexpensive synthesis of the novel and molecular hole transport material **CPDA 1**, which is based on a common cyclopentadiene dimethyl acetale core and substituted by four triarylamine moieties in a star-shaped fashion. Structural details and packing motifs of **CPDA 1** in the solid state were elucidated by single crystal X-ray structure analysis and gave insight into the packing motifs of the molecules in the solid state. Besides high thermal stability, the glass transition temperature and melting point of films of **CPDA 1** are only marginally influenced by addition of additives, which are typically used for improved hole mobility and good photovoltaic performance in perovskite solar cells. Together with the favorable optoelectronic and transport properties, high power conversion efficiency of 23.1% in n-i-p PSCs is achieved which is among the highest reported to date. "Gold standard" spiro-OMeTAD was surpassed in some metrics, among them straightforward inexpensive synthesis, higher efficiency, smaller hysteresis of the *J-V* curves, and substantially higher long-term stability in PSCs. Furthermore, our novel HTM allowed for better charge extraction, transport, and separation compared to spiro-OMeTAD which was indicated by transient and steady state emission. In the light of these results, we believe that our work opens up a new pathway for developing inexpensive hole-transport materials that show the potential to further push the performance of PSCs while retaining their operational stability.

Supporting Information

Supporting Information is available from the Wiley Online Library or from the authors. All experimental details, materials, methods, synthesis, NMR and HRMS spectra, cost estimation, single crystal X-ray structure analysis, thermal and optical properties, ToF and SCLC mobility and solar cell measurements are given in the Supporting Information.

Acknowledgements

H.Z. thanks the China Scholarship Council for funding. Y.L., S.M.Z., and M.G. thank the King Abdulaziz City for Science and Technology (KACST) and the European Union's Horizon 2020 research and innovation program (grant agreement No 826013) for financial support. F.T.E. acknowledges financial support from the Swiss National Science Foundation R'Equip program under the grant number 183305. University of Cologne acknowledges the project ASTRAL sponsored by the German Science Foundation (DFG)

as well as the cluster “Quantum Matter and Materials (QM2)” at the University of Cologne for financial support.

Conflicts of interest

There are no conflicts to declare.

Keywords

Cyclopentadiene acetale, low-cost hole transport material, long-term stability, perovskite solar cell, high efficiency, X-ray structure analysis

References

1 Y. Wang, T. Wu, J. Barbaud, W. Kong, D. Cui, H. Chen, X. Yang, L. Han, X. Yang, L. Hanand, L. Han, *Science,* **2019**, *365*, 687.
2 E. H. Jung, N. J. Jeon, E. Y. Park, C. S. Moon, T.-Y. Yang, J. H. Noh, J. Seo, C. S. Moon, J. H. Noh, T. J. Shin, *Nature,* **2019**, *567*, 511-515.
3 S. Bai, P. Da, C. Li, Z. Wang, Z. Yuan, F. Fu, M. Kawecki, X. Liu, N. Sakai, J. T.-W. Wang, S. Huettner, S. Buecheler, M. Fahlman, F. Gao, H. J. Snaith, *Nature,* **2019**, *571*, 245-250.
4 H. Zhu, Y. Liu, F. T. Eickemeyer, L. Pan, D. Ren, M. A. Ruiz-Preciado, B. Carlsen, B. Yang, X. Dong, Z. Wang, H. Liu, S. Wang, S. M. Zakeeruddin, A. Hagfeldt, M. I. Dar, X. Li, M. Grätzel, *Adv. Mater.* **2020**, *32*, 1907757.
5 A. Miyata, A. Mitioglu, P. Plochocka, O. Portugall, J. T.-W. Wang, S. D. Stranks, H. J. Snaith, R. J. Nicholas, *Nat. Phys.,* **2015**, *11*, 582-587.
6 S. D. Stranks, G. E. Eperon, G. Grancini, C. Menelaou, M. J. P. Alcocer, T. Leijtens, L. M. Herz, A. Petrozza, H. J. Snaith, *Science,* **2013**, *342*, 341-344.
7 A. Kojima, K. Teshima, Y. Shirai, T. Miyasaka, *J. Am. Chem. Soc*., **2009**, *131*, 6050-6051.
8 M. Jeong, I. W. Choi, E. M. Go, Y. Cho, M. Kim, B. Lee, S. Jeong, Y. Jo, H. W. Choi, J. Lee, J.-H. Bae, S. K. Kwak, D. S. Kim, C. Yang, *Science,* **2020**, *369*, 1615-1620.
9 N.-G. Park, *ACS Energy Lett.,* **2019**, *4*, 2983-2985.
10 J. Melas-Kyriazi, I. K. Ding, A. Marchioro, A. Punzi, B. E. Hardin, G. F. Burkhard, N. Tétreault, M. Grätzel, J.-E. Moser, M. D. McGehee, *Adv. Energy Mater.,* **2011**, *1*, 407-414.
11 Y.-K. Wang, Z.-C. Yuan, G.-Z. Shi, Y.-X. Li, Q. Li, F. Hui, B.-Q. Sun, Z.-Q. Jiang, L.-S. Liao, *Adv. Funct. Mater.,* **2016**, *26*, 1375-1381.
12 G.-W. Kim, H. Choi, M. Kim, J. Lee, S. Y. Son, T. Park, *Adv. Energy Mater*., **2020**, *10*, 1903403.
13 H. D. Pham, T. C.-j. Yang, S. M. Jain, G. J. Wilson, P. Sonar, *Adv. Energy Mater*., **2020**, *10*, 1903326.
14 J. Urieta-Mora, I. Garvica-Benito, A. Molina-Ontoria, N. Martin, *Chem. Soc. Rev*., **2018**, *47*, 8541-8571.
15 U. Bach, D. Lupo, P. Comte, J. E. Moser, F. Weissörtel, J. Salbeck, H. Spreitzer, M. Grätzel, *Nature,* **1998**, *395*, 583-585.
16 H.-S. Kim, J.-Y. Seo, S. Akin, E. Simon, M. Fleischer, S. M. Zakeeruddin, M. Grätzel, A. Hagfeldt, *Nano Energy* **2019**, *61*, 126-131.
17 X. Liu, F. Zhang, Z. Liu, Y. Xiao, S. Wang, X. Li, *J. Mater. Chem. C*, **2017**, *5*, 11429-11435.
18 M. Kim, G.-H. Kim, T. K. Lee, I. W. Choi, H. W. Choi, Y. Jo, Y. J. Yoon, J. W. Kim, J. Lee, D. Huh, H. Lee, S. K. Kwak, J. Y. Kim, D. S. Kim, *Joule*, **2019**, *3*, 1-14.
19 N. J. Jeon, H. Na, E. H. Jung, T.-Y. Yang, Y. G. Lee, G. Kim, H.-W. Shin, S. I. Seok, J. Lee, J. Seo, *Nat. Energy*, **2018**, *3*, 682-689.

20 S. Akin, M. Bauer, R. Uchida, N. Arora, G. Jacopin, Y. Liu, D. Hertel, K. Meerholz, E. Mena-Osteritz, P. Bäuerle, S. M. Zakeeruddin, M. I. Dar, M. Grätzel, *ACS Appl. Energy Mater.*, **2020**, *3*, 7456-7463.
21 X.-J. Ma, X.-D. Zhu, K.-L. Wang, F. Igbari, Y. Yuan, Y. Zhang, C.-H. Gao, Z.-Q. Jiang, Z.-K. Wang, L.-S. Liao, *Nano Energy*, **2019**, *63*, 103865.
22 Y. Wang, Q. Liao, J. Chen, W. Huang, X. Zhuang, Y. Tang, B. Li, X. Yao, X. Feng, X. Zhang, M. Su, Z. He, T. J. Marks, A. Facchetti, X. Guo, *J. Am. Chem. Soc*., **2020**, on-line (doi.org/10.1021/jacs.0c06373).
23 T. Malinauskas, D. Tomkute-Luksiene, R. Sens, M. Daskeviciene, R. Send, H. Wonneberger, V. Jankauskas, I. Bruder, V. Getautis, *ACS Appl. Mater. Interf.* **2015**, *7*, 11107-11116.
24 H. Li, C. Lambert, *Chem. Eur. J*., **2006**, *12*, 1144-1155.
25 S. Barlow, C. Risko, S.-J. Chung, N. M. Tucker, V. Coropceanu, S. C. Jones, Z. Levi, J.-L. Brédas, S. R. Marder, *J. Am. Chem. Soc*., **2005**, *127*, 16900-16911.
26 W. Lilienblum, R. W. Hoffmann, *Chem. Ber*., **1977**, *110*, 3405-3409.
27 H. Dürr, R. Gleiter, *Angew. Chem. Int. Ed*., **1978**, *17*, 559-569.
28 C. M. Cardona, W. Li, A. E. Kaifer, D. Stockdale, G. C. Bazan, *Adv. Mater.*, **2011**, *23*, 2367-2371.
29 D. Poplavskyy, J. Nelson, *J. Appl. Phys*. **2003**, *93*, 341-346.
30 T. Kirchartz, J. A. Márquez, M. Stolterfoht, T. Unold, *Adv. Energy Mater*., **2020**, 1904134.